Journal of Alloys and Compounds 794 (2019) 120–126

Contents lists available at ScienceDirect

Journal of Alloys and Compounds

journal homepage: http://www.elsevier.com/locate/jalcom

Improving performance in ytterbium-erbium doped waveguide amplifiers through scattering by large silicon nanostructures

Niklaus Ursus Wetter [a, *], Diego Silverio da Silva [b], Luciana Reyes Pires Kassab [c], Ernesto Jimenez-Villar [a]

[a] Centro de Lasers e Aplicações, Instituto de Pesquisas Energéticas e Nucleares CNEN-IPEN/SP, Av. Prof. Lineu Prestes 2242, São Paulo, CEP 05508-000, Brazil
[b] Escola Politécnica, Universidade de São Paulo, 05508-970, São Paulo, Brazil
[c] Faculdade de Tecnologia de São Paulo, CEETEPS/UNESP, 01124-060, São Paulo, Brazil

ARTICLE INFO

Article history:
Received 13 March 2019
Received in revised form
11 April 2019
Accepted 13 April 2019
Available online 16 April 2019

Keywords:
Optical materials
Sputtering
Optical properties

ABSTRACT

Optical waveguide amplifiers have seen a growing interest in the last years due to their applications in telecommunication. This paper reports a notable increase of the relative gain of Yb^{3+}/Er^{3+} codoped Bi_2O_3–GeO_2 waveguides by introducing disorder in the form of silicon nanostructure as scattering centers. A photoluminescence enhancement of about 10 times for the 520 nm and 1530 nm emission bands is observed in the waveguides when the silicon nanostructures are introduced. Increase of the Yb^{3+}/Er^{3+} effective absorption, due to the scattering provided by the silicon nanostructures, and decrease of $[Bi^{+}]$, caused by the introduction of silicon, are proposed as likely causes for the luminescence and gain enhancement. The pedestal waveguides were fabricated by RF-sputtering followed by optical lithography and reactive ion etching. RF-sputtering of silicon together with Yb/Er and Bi_2O_3–GeO_2 glass, followed by heat treatment, produced Yb^{3+}/Er^{3+} codoped Bi_2O_3–GeO_2 waveguides with silicon nanostructures of size 25–30 nm. The resulting relative gain reached 5.5 dB/cm at 1542 nm representing an enhancement of 50% with respect to waveguides without silicon nanostructures. This strategy of introducing appropriate disorder may open an avenue for designing and manufacture of novel photonic devices in this emerging field of integrated optics.

1. Introduction

Since the invention of erbium doped optical fiber amplifiers (EDFAs) scientists have invested heavily into researching new Er^{3+} doped materials for the production of evermore efficient devices for optical amplifiers and fiber networks used in the telecommunication window at 1.5 μm. Photoluminescence enhancement (PE) of materials doped with rare earth (RE) ions and metallic nanoparticles (gold or silver) has been reported for applications in photonic devices such as color displays, lasers and optical amplifiers [1–3]. In these experiments, the enhancement was attributed to an increased local field in the vicinity of the metallic nanoparticles enhancing the photoluminescence (PL) of the RE ions [4]. The use of semiconductor nanocrystals (quantum dots) represents another alternative for PL enhancement because their absorption cross sections are normally larger than the rare earth ions cross sections [1,5]. The energy transfer process to the RE ions can be made very efficient by controlling the size of the quantum dots allowing thereby to match their energy gap to the radiative transitions of the RE ions. Examples of Er^{3+} PL enhancement include mostly silicate thin films and waveguide devices with silicon nanocrystals prepared by using different techniques such as ion implantation, lithography, chemical vapor deposition and sputtering technique [5]. Optimization of waveguides amplifiers based on Er^{3+} doped silicate thin films with silicon nanocrystals were also reported [6].

The investigation of new materials is not only motivated by the search for better PL efficiency, but also by applications requiring higher refractive index for more nonlinear response and higher index contrast, such as waveguide amplifiers. Heavy metal oxide materials represent a good alternative because of their larger linear refractive index (~2.0), high nonlinear response and smaller cutoff phonon energy (500-700 cm^{-1}) [7,8]. Compared to the well-known production technique of silica glasses for optical fibers and planar waveguides, there is a general lack of literature related to research

* Corresponding author.
E-mail address: nuwetter@ipen.br (N.U. Wetter).

https://doi.org/10.1016/j.jallcom.2019.04.141
0925-8388/

on heavy metal oxide glasses incorporating silicon nanostructures (NSs). PL enhancements in Er^{3+} doped germanate glasses (Bi_2O_3–GeO_2) due to the presence of silicon nanocrystals with size larger than 10 nm has been demonstrated elsewhere [9]. Growth of ~200% in the Er^{3+} emission at 545 nm and ~100% at 525 nm, 660 nm and 1530 nm has also been shown [9]. Quenching of the luminescence was observed for large concentration of silicon nanocrystals, mainly in the near infrared region. PL enhancement of approximately 300% in the presence of Si nanocrystals was reported for tellurite glasses (TeO_2-ZnO) doped with Er^{3+}, in the visible and near infrared regions [10]. In both cases, the glasses were produced using the melting-quenching technique followed by adequate thermal annealing to control the nucleation of silicon nanocrystals. Increased optical gain of 7 dB/cm at 1535 nm was demonstrated in an Er^{3+} doped silicon–rich, silicon-oxide waveguide amplifier containing Si nanocrystals [6]. However, in these works, the scattering property of silicon NSs and its influence on the waveguide performance was not addressed. In recent years, there has been a dramatic progress in the photonics field in disordered optical media, ranging from applications in random lasers and other novel photonic functions [11–16], to investigations into fundamental topics, such as localization of light [17–21]. Disorder in optical systems, which, until recently, was thought of as hampering system performance and avoided at all costs, has given rise to new and interesting phenomena in photonic crystals [22–25].

In this work, we pursue a new strategy of PL enhancement in Yb^{3+}/Er^{3+} codoped Bi_2O_3–GeO_2 waveguides, which is provided through disorder or scattering. It is well known that the introduction of scattering (relatively large nanoparticles with high contrast of refractive index, like TiO_2 or Si nanoparticles) in an optical system can increase notably the effective optical path length, which leads to an increase of the effective absorption and luminescence [12–20]. In addition, Si NSs (high refractive index ~3.7) in a waveguide at high concentration must increase the effective refractive index, which should improve the waveguide performance. These ideas motivated the present study of the performance of Yb^{3+}/Er^{3+} codoped Bi_2O_3–GeO_2 waveguides with Si NSs for amplification at 1542 nm. We demonstrate the possibility to produce Si NSs (25–30 nm size) using the sputtering technique followed by an adequate heat treatment avoiding the use of more complex processes. As a result, we achieve a PL enhancement of approximately ten times at 520 nm and 1530 nm and a 50% increase of the relative gain at 1542 nm, for a waveguide of 10 mm length. These results were attributed to two main factors: i) increase of the effective absorption and gain of RE by the increase of the effective optical path length, which is induced through the elastic scattering provided by the Si scatterer nanostructures (25–30 nm diameter); ii) $[Bi^+]$ decrease by silicon that induces Bi oxidation ($Bi^+ \rightarrow Bi^{2+}$, Bi^{3+}), which reduces optical losses at the pump wavelength of 980 nm.

2. Experimental

Conventional microelectronics fabrication techniques were used to produce the Yb^{3+}/Er^{3+} codoped Bi_2O_3-GeO_2 (BGO) pedestal waveguides, with and without Si NSs, following the sequence shown elsewhere [26]. Yb^{3+}/Er^{3+} codoped BGO thin films were produced using RF magnetron sputtering. High resolution transmission electron microscopy (HR-TEM), electron diffraction pattern (EDP) analysis, energy dispersive spectroscopy (EDS) and small angle X ray scattering (SAXS) were performed in order to obtain information about the morphology and structure of the silicon NSs. Concentrations of RE ions, Bi and Si were determined by Rutherford backscattering spectrometry (RBS) and particle induced X-ray emission (PIXE) analysis following studies of Miritello [27]. Scanning Electron Microscopy (SEM) was performed to analyze the pedestal profile. The concentrations of Er^{3+} and Yb^{3+} ions in both samples, with and without Si NSs, were $[Er^{3+}] = 1.34E21$ at/cm^3, $[Yb^{3+}] = 3.90E21$ at/cm^3 and $[Er^{3+}] = 1.00E21$ at/cm^3, $[Yb^{3+}] = 2.76E21$ at/cm^3 respectively. The ballistic absorption lengths (l_a) estimated for these Er^{3+} and Yb^{3+} concentrations at 980 nm in the samples with and without Si NSs are $l_a(Er^{3+}) = 3.1$ mm, $l_a(Yb^{3+}) = 0.2$ mm and $l_a(Er^{3+}) = 4.2$ mm, $l_a(Yb^{3+}) = 0.23$ mm, respectively. The Bi concentrations in the waveguides with and without Si NSs are 7.8% and 8.3%, respectively. The Si stoichiometric percentage determined by RBS was (1.7 ± 0.12)%.

The 980 nm pump absorption and 1530 nm fluorescence spectra at very low pump powers were collected from the top of the waveguide (Fig. 1(a)) as a function of the longitudinal distance from the waveguide pump facet using a 200 μm diameter fiber, coupled to a spectrometer, in close proximity to the top surface.

The relative gain at 1542 nm was measured using 980 nm and 1542 nm for pump and signal wavelengths, respectively. The value of the relative gain is given by the ratio of the signal peak with and without 980 nm pumping [28].For the measurements, both wavelengths are multiplexed inside a waveguide division multiplexer (WDM) and coupled into the pedestal waveguides using single mode fibers. The signal power injected into the waveguides (Fig. 1(b)) was kept low to prevent gain saturation and fixed in all experiments to 20 μW. The output signal was also collected by an optical fiber at the end of the waveguide and sent to an optical spectrum analyzer, in order to evaluate the gain.

3. Results and discussions

Fig. 1 c) and d) show scanning electron microscopy (SEM) images of an Er^{3+}/Yb^{3+} codoped BGO pedestal waveguide with 500 nm height, which was the height that promoted the smallest propagation loss in a group of samples with different thin film

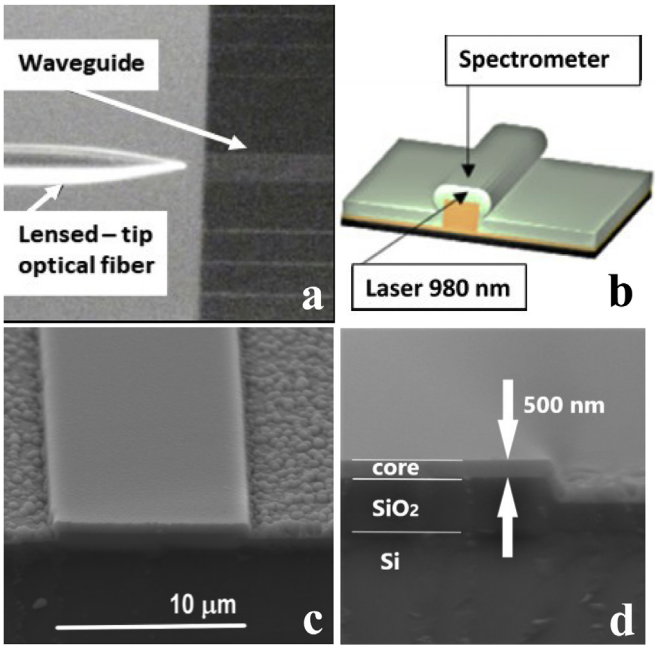

Fig. 1. (a) Top view microscopy image showing the lensed-tip fiber optic and the waveguide. (b) Illustration of the set-up for measuring scattered light at 980 nm and 1530 nm from the waveguide. (c) and (d) are SEM images of the Er^{3+}/Yb^{3+} codoped BGO pedestal waveguide. (c) Top view of a waveguide of 10 μm width and 500 nm height. c) front view showing waveguide core dimensions.

thicknesses, varying from 300 to 1000 nm. Fig. 2 shows HR-TEM images of the Yb^{3+}/Er^{3+} codoped BGO thin film (waveguide) prepared with Si. Silicon NSs, which are inferred by the EDS local analysis, are observed with size of around 25–35 nm. This kind of Si NSs can behave as a source of scattering, due to the high refractive index of Si (~3.7). Electron diffraction pattern [29], energy dispersive spectroscopy (EDS) and small angle X ray scattering (SAXS) confirmed that these NSs are composed of silicon.

The PL spectra of the Yb^{3+}/Er^{3+} codoped BGO thin films with and without Si NSs, resulting in near infrared (NIR) to infrared frequency down-conversion and NIR to visible up-conversion, are shown in Fig. 3 (980 nm excitation). An enhancement of the PL peak intensities of 7 and 10 times for $\lambda = 530$ nm and $\lambda = 1530$ nm, respectively, is observed in the waveguide containing Si NSs. Also observed is the emission at 1200 nm from the Bi^{+} ions, which decreases 50% in the presence of Si NSs. However, [Bi], determined by RBS, in the waveguide with Si NSs is only 6% lower than that in the waveguide without Si NSs, which indicates an appreciable decrease in the $[Bi^{+}]/[Bi]$ ratio.

Normally Bi^{+} absorbs the energy at 980 nm and emits at 1200 nm [30]. The deposition of the BGO thin film with silicon using the sputtering technique, can lead to the incorporation of Si^{+} species in the as-deposited BGO glass. These Si^{+} ions would be reduced to form Si nanocrystals during thermal annealing, oxidizing Bi^{+} to Bi^{3+} ($2Si^{+} + Bi^{+} \leftrightarrow 2Si + Bi^{3+}$). Thereby, the $[Bi^{+}]/[Bi]$ ratio decreases causing a luminescence decrease at ~1200 nm. A similar effect has been reported in the presence of CeO_2, where Ce^{4+} is reduced to Ce^{3+}, oxidizing Bi^{+} to Bi^{3+} [31].

The large PL increase at 1530 nm in the Si-nanostructures doped waveguide may be attributed to three main effects: i) increase of the effective optical path length due to the scattering provided by the Si NSs, leading to an absorption increase of Yb^{3+} ions; ii) decrease of $[Bi^{+}]$ and its respective absorption band (980 nm), increasing the effective pumping intensity for the Yb^{3+} ions inside the waveguide and iii) smaller reabsorption at 1542 nm due to the decrease of $[Bi^{+}]$ and resulting decrease of $Er^{3+} \rightarrow Bi^{+}$ energy back-transfer [32]. The measured radiative lifetimes of the PL bands centered at 550 nm and 1530 nm for the samples without Si nanostructure are 28.9 μs and 5.81 ms, respectively. For the samples with Si nanostructure, the respective lifetimes are 21.8 μs and 5.5 ms. The lifetimes of Er^{3+} are similar which could be an indication that the higher Yb^{3+}/Er^{3+} doping concentration of the waveguide with Si (30% higher) causes approximately a similar reduction in lifetime as the increased $Er^{3+} \rightarrow Bi^{+}$ energy back-transfer of the waveguide without Si. Calculated emission cross sections for the PL spectra presented in Fig. 3(b) are 4×10^{-21} cm^2 at 1530 nm for both waveguides, calculated by applying the Füchtbauer-Ladenburg equation to the luminescence spectrum and using the measured luminescence decay time of 5.5 ms [33].

The Si filling fraction was estimated at ~4.7% (volume), which was determined considering the results obtained from RBS for the chemical composition (1.7 ± 0.12)% and the densities of the germanate host (6.2 g/cm^3) and Si nanocrystals (2.3 g/cm^3 for cubic structure). Si NSs at this filling fraction cause an increase of the effective refractive index of the waveguides. The refractive index was determined as described in Ref. [34] and we obtained 1.9 and 1.88 for the pumping wavelength (980 nm) and 1.9 and 1.77 for the signal (1542 nm) of the thin film with and without Si, respectively. The higher refractive index of the Si containing waveguide should induce a decrease of the intrinsic losses of BGO waveguides at 1542 nm associated to the irregular morphology or defects at the waveguide borders. However, owing to the Si NSs that behave as a source of scattering, these may induce additional losses. Additionally, the Si NSs should also provide inelastic scattering (absorption) at 980 nm (pumping), but at 1542 nm (gain) the absorption values should be small compared to shorter wavelengths. Considering Si NSs of around 30 nm diameter (as are observed in the TEM image, see Fig. 2) at a filling fraction of 4.7%, the transport mean free paths (l_T), calculated by MIE theory [35], yield ~0.8 mm and ~5 mm for 980 nm and 1542 nm wavelengths, respectively. This induces an increase of the effective optical path length mainly for the pumping wavelength (980 nm) as represented in Fig. 4(a). Consequently, an increase of the effective absorption by Yb^{3+} (980 nm), luminescence and gain by Er^{3+} (1542 nm) should be expected.

In order to determine the expected enhancement of absorption and luminescence, pump absorption (980 nm) and fluorescence spectra (1530 nm) at very low pump powers (passive regime) were collected from the top as a function of the longitudinal distance from the pump facet. For both waveguides with and without Si NSs, the peak intensity at 980 nm (pumping) and 1530 nm (fluorescence) are displayed in Fig. 4 b and c, respectively. As is expected for low pump powers, the exponential decay factors at 980 nm and 1530 nm are the same for both waveguides, since luminescence must be proportional to pumping intensity. The decay behavior at 980 nm and 1530 nm can be expressed by equations (1) and (2), respectively:

$$I_{980}(d) = kI_{980}(0)e^{-\frac{d}{D}} \quad (1)$$

$$I_{1530}(d) = fI_{980}(d)\sigma n \quad (2)$$

Where the constant k includes the waveguide coupling losses and the detection factor at 980 nm and f is a detection factor at 1530 nm, $I_{980}(0)$ is the pump power at the waveguide's input facet, $I_{1530}(d)$ is the signal power at position d inside the waveguide, D is the decay

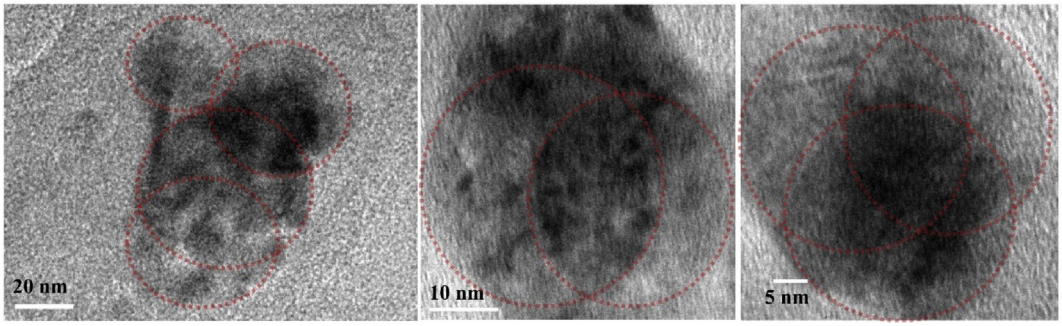

Fig. 2. HR-TEM images of the thin film waveguide containing Si nanostructures (500 nm thickness). Si aggregates with 25–35 nm size are observed. Dashed red lines were introduced for highlighting of the contours of Si aggregates. The scale bar is shown in each image. (For interpretation of the references to color in this figure legend, the reader is referred to the Web version of this article.)

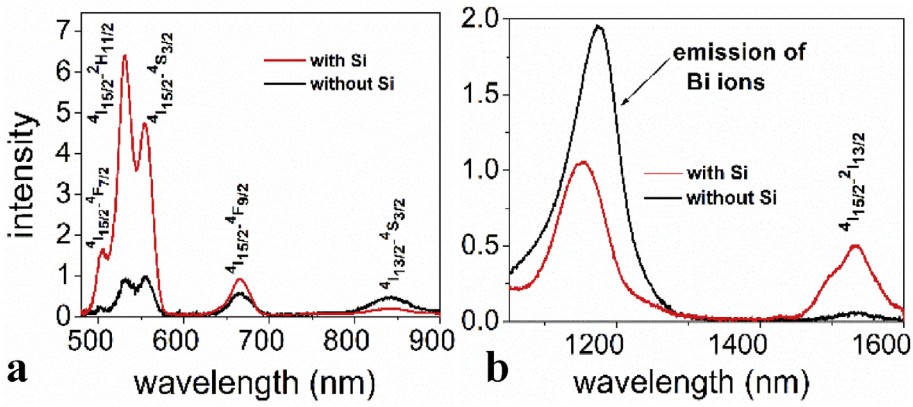

Fig. 3. PL spectra of Er3+/Yb3+ codoped BGO thin films, normalized to the waveguide with Si, under excitation at 980 nm in (a) the visible and (b) the near infrared region.

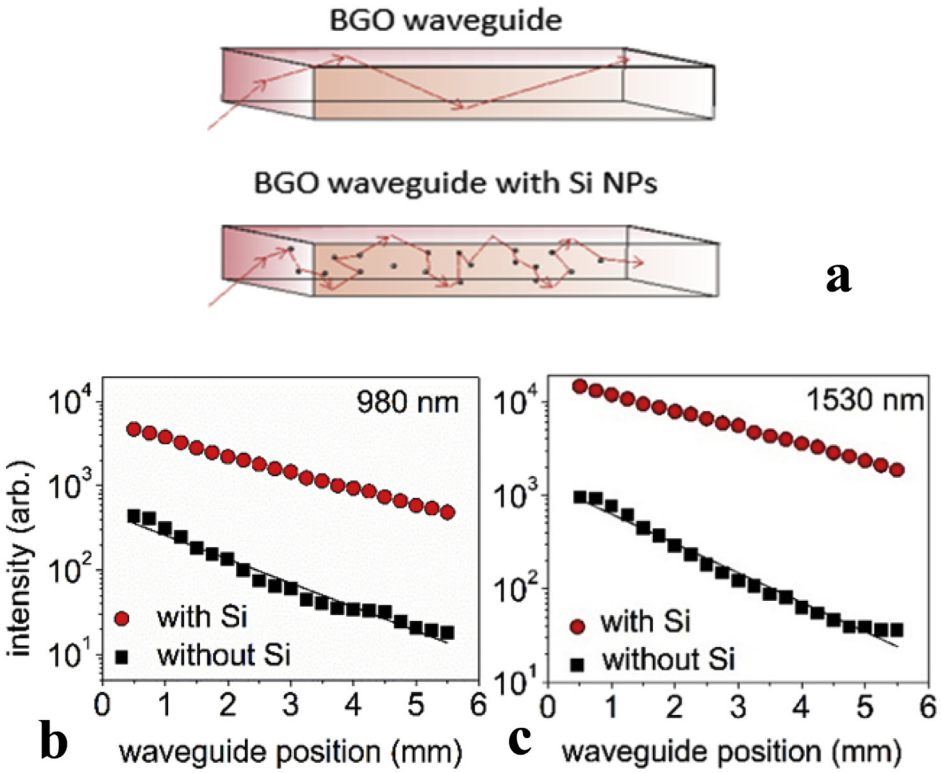

Fig. 4. a) Schematic view of the increase of optical path-length in a waveguide with Si nanostructures (scatterers) in comparison with one without Si nanostructures. b-c) low pump power luminescence intensity (passive regime) in log scale for both types of waveguides, measured outside and perpendicular to the top surface of waveguides, as a function of the longitudinal waveguide position, b) measured at 980 nm and c) measured at 1530 nm.

factor due to Yb^{3+} and Bi^{+} absorption including distributed waveguide losses in general, σ is the effective absorption cross section for Yb^{3+} and n is the [Yb^{3+}]. Here we have neglected absorption from Er^{3+} given its comparably smaller doping level and more than one order of magnitude smaller absorption cross section. The measured exponential decay factors at 980 nm and 1530 nm are $D_C = 1.2$ mm and $D_S = 2.5$ mm for the waveguides with (c) and without (s) Si NSs, respectively. The smaller decay factor of the waveguide with Si NSs indicates a decrease in the waveguide losses which can be attributed to i) decrease of [Bi^{+}] and ii) higher effective index of refraction of the waveguide due to the presence of Si NSs.

As we shall demonstrate below, we can isolate the contribution of absorption increase by scattering from the other effects and calculate its contribution. When observing the relative intensities in Fig. 4(b) and c, we observe higher intensities for the waveguide with Si NSs. Note that we have shown that due to Si NSs there is an increase in the scattering strength at 980 nm many times bigger when compared to 1530 nm. The division of both spectra generates a constant value of $I_C(1530\,nm)/I_C(980\,nm) = 3.7$ and $I_S(1530\,nm)/I_S(980\,nm) = 2.1$, respectively. The division of both spectra, made possible by the linear dependency of I_{1530} with I_{980}, eliminates the need to consider individual Bi^{+} absorption and waveguide passive losses or geometrical factors (such as k and f) and allows to establish an equation (equation (3)) that depends on the concentration ratio of Yb^{3+}, f_n, and on the ratio of the effective absorption

cross sections of the waveguides, f_σ, with and without Si NSs.

$$\frac{I_c^{1530}}{I_c^{980}} = \frac{I_s^{1530}}{I_s^{980}} f_\sigma f_n \tag{3}$$

The concentration ratio of Yb^{3+}, $f_n = [Yb_c^{3+}]/[Yb_s^{3+}]$, is equal to 1.4. As a result of the calculation, we obtained a value of $f_\sigma = 1.26 \pm 0.12$, which corresponds to an effective increase of the Yb^{3+} cross section of the waveguide with Si NSs of 26%. Therefore, this increase is ascribed solely to the disorder or scattering effect provided by the NSs and represents the central findings of this work.

The increase in effective absorption cross-section implies in a similar decrease of the effective Yb^{3+} absorption length (macroscopic absorption), l_{MA}. The macroscopic absorption length (l_{MA}) can be determined in the presence of scattering by the expression $1/l_{MA} = 1/l_a + 1/l_T$, where l_a and l_T are the microscopic or ballistic absorption length and the transport mean free path associated to the scattering, respectively. From the absorption increase we extract an experimental value of $l_T \approx 790\ \mu m$, which agrees satisfactorily with the transport mean free path estimated at 980 nm from silicon NSs of diameters around 25–30 nm with an estimated filling fraction of 4.7% suspended within a matrix with 1.9 refractive index, as calculated by Mie theory. This also indicates that the effective absorption increase is not achieved by photon trapping but due to a longer photon path length inside the waveguide.

The waveguide amplifier performance is shown in Fig. 5. Fig. 5(a) shows the emission spectra without and with pumping (excitation at 980 nm) of the waveguide with Si NSs. Fig. 5(b) and (c) shows the relative gain at 1542 nm of Er^{3+}/Yb^{3+} codoped BGO pedestal waveguides with dimensions 100 μm × 1 cm (width x length) and 500 nm core height, with and without Si nanostructure, as a function of pump power at 980 nm. The relative gain is defined as $10\ \log[I_P(\lambda)/I_u(\lambda)]$, where $I_P(\lambda)$ and $I_u(\lambda)$ are the signal intensities (1542 nm) for the pumped and unpumped case, respectively. Fig. 5(b) shows the relative gain measured at the top of the waveguide at a fixed position of 2 mm. Similar results are observed for measurements taken at 1.5 mm and 3 mm. The behavior of Er^{3+}/Yb^{3+} waveguide has been treated extensively in the literature and their behavior as a function of $[Er^{3+}]$, $[Yb^{3+}]$ and waveguide length for different pump powers at 980 nm has been analyzed [36]. The performance can be summarized as follows: below the saturation pump power, the waveguide output power at 1542 nm decreases continuously and almost linearly as a function of $[Yb^{3+}]$. The higher the Yb^{3+} concentration the higher the pump power necessary to saturate the waveguide and therefore the smaller the slope efficiency for a given waveguide length. Once saturated, the output power depends only on $[Er^{3+}]$ for a given waveguide length.

The waveguide with Si NSs has a 1.4x higher Yb^{3+} concentration and therefore should have a smaller slope efficiency. However, clearly seen in Fig. 5(b) is the higher slope of the waveguide with Si NSs at lower pump powers and before the saturation. The result can be explained by the higher effective cross-section of the waveguide with Si NSs (1.26 times). Fig. 5(c) shows the gain at the output of the 1 cm long waveguide. At the maximum pump power of 60 mW, relative gains of 5.35 e 3.75 dB/cm were measured for waveguides with and without Si NSs, respectively.

We remark that the fabrication parameters of the waveguides can be exploited to optimize the gain performance (stimulated emission phenomena). For example, the waveguide length can be diminished such that it would be slightly longer than the effective absorption length (l_{MA}). The decay of the pumping intensity (980 nm), $I(d)$, by absorbed energy in this waveguide with scattering (Si NSs) can be expressed as (equation (4)):

$$I(d) = e^{-\left(\frac{d}{l_{MA}}\right)} \tag{4}$$

where d represents the waveguide length. A l_T value around l_a would lead to an appreciable increase of absorbed energy in the waveguide. A similar mechanism must occur for the gain above threshold. Clearly, d must be around or slightly larger than l_{MA} in order to reach the gain threshold in the whole waveguide extension. Notice that if $l_{MA} \ll d$ the deeper waveguide part can be below the gain threshold, which would provoke energy re-absorption and, consequently, a decrease of total gain. An increase of pumping intensity would then lead to absorption saturation at the beginning of the waveguide and population inversion over the whole waveguide extension. This would explain why the relative gain, measured at 2 mm depth (1542 nm), was further enhanced by 100% and reached 6.2 dB/cm. Additionally, this could be the motive of the second slope efficiency seen at position of 2 mm (Fig. 5(b)), starting at approximately 20 mW of pump power.

We recall that the Si NSs (25–30 nm) do not present quantum confinement and their indirect energy bandgap does not differ from the bandgap of bulk silicon (1.12eV) [10,37]. In addition, from the lower filling fraction of Si (4.7%) together with the size of the Si NSs, we can infer that the percentage of Er^{3+}/Yb^{3+} near Si NSs (nearer than 5 nm) is low and excludes an appreciable energy transference. In other words, the energy transfer mechanism from Si NSs to Er^{3+} and/or to Yb^{3+} followed by energy transfer to Er^{3+} located in its proximity should not be appreciable. Thereby, the resonant excitation of Er^{3+} and Yb^{3+} must be the likely mechanism of Er^{3+} excitation.

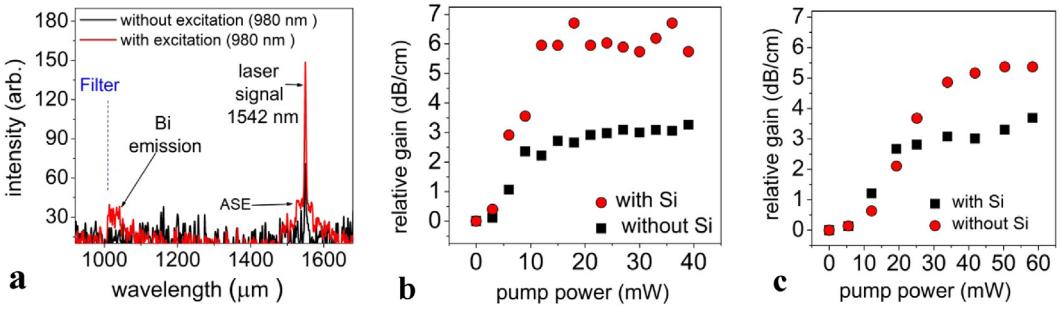

Fig. 5. (a) Emission spectra, with and without excitation at 980 nm, collected during gain measurements of the waveguides (100 μm width) with Si nanostructures. b-c) For the waveguides with and without Si nanostructures: relative gain as a function of the pump power at (b) a fixed position of 2 mm measured from the top of the waveguide and (c) measured at the exit facet (10 mm).

4. Conclusions

This paper shows the notable influence of the disorder (Si nanostructures) on optical properties (absorption, luminescence and gain) of the Yb^{3+}/Er^{3+} codoped Bi_2O_3-GeO_2 pedestal waveguides. A method for producing Si nanostructures using the RF-sputtering technique followed by an adequate heat treatment is presented in this work. The relative gain, measured at 1542 nm, was enhanced by 50% and reached 5.5 dB/cm. Large PL enhancement (~10 times) was observed in the visible and infrared regions. These facts have been attributed to an increase of the effective energy absorbed by the rare earths due to two main factors: i) an increase of the optical path length due to the scattering provided by the Si nanostructures, which leads to an increase of the effective Yb^{3+} cross-section (absorption); ii) the increase of the effective pumping intensity due to the decrease of [Bi^{+}] absorption and the waveguide losses (higher refraction index). The experimentally determined increase in effective absorption cross-section due to the scattering effect alone is 26%. The increase of the refractive index of the BGO waveguide (1542 nm) by the Si presence should also increase the amount of waveguide modes. This strategy of introducing appropriate amount of disorder (Si nanostructures) in a waveguide can open a way for manufacturing more efficient amplifier waveguides and other advanced photonic devices. These results open new possibilities for pedestal waveguides fabrication and its application in integrated optics.

Author contributions

D.S.D.S. performed the experiments; all authors participated in analyzing the results and writing the manuscript.

Funding sources

This work received grants from the Brazilian National Council for Scientific and Technological Development CNPq (grant 465.763/2014) and the São Paulo State Science Foundation FAPESP (grants PV-2017/05854-9 and 2013/26113-6).

Acknowledgment

We acknowledge the Polytechnical School of the University of São Paulo (POLI/USP) for the collaboration during the waveguide fabrication and the National Laboratory for Nanotechnology (LNNano)/CNPEM for HR-TEM measurements.

References

[1] Y.L. Tupei Chen, Semiconductor, Nanocrystals and Metal Nanoparticles: Physical Properties and Device Applications, CRC Press, 2016.
[2] C.B. de Araujo, D.S. da Silva, T.A.A. de Assumpção, L.R.P. Kassab, D.M. da Silva, Enhanced optical properties of germanate and tellurite glasses containing metal or semiconductor nanoparticles, Sci. World J. 2013 (2013) 1–13, https://doi.org/10.1155/2013/385193.
[3] L.R.P. Kassab, D.M. Silva, J.A.M. Garcia, D.S. da Silva, C.B. de Araújo, Silver nanoparticles enhanced photoluminescence of Nd3+doped germanate glasses at 1064 nm, Opt. Mater. (Amst.) 60 (2016) 25–29, https://doi.org/10.1016/j.optmat.2016.07.006.
[4] P.N. Prasad, Nanophotonics, John Wiley & Sons, Inc., 2004, https://doi.org/10.1002/0471670251.
[5] N. Koshida (Ed.), Device Applications of Silicon Nanocrystals and Nanostructures, Springer {US}, 2009, https://doi.org/10.1007/978-0-387-78689-6.
[6] H.-S. Han, S.-Y. Seo, J.H. Shin, N. Park, Coefficient determination related to optical gain in erbium-doped silicon-rich silicon oxide waveguide amplifier, Appl. Phys. Lett. 81 (2002) 3720–3722, https://doi.org/10.1063/1.1520710.
[7] L.R.P. Kassab, M.E. Fukumoto, V.D.D. Cacho, N.U. Wetter, N.I. Morimoto, Spectroscopic properties of Yb3+doped PbO-Bi2O3-Ga2O3glasses for IR laser applications, Opt. Mater. (Amst.) 27 (2005) 1576–1582, https://doi.org/10.1016/j.optmat.2005.04.006.
[8] F.A. Bomfim, J.R. Martinelli, L.R.P. Kassab, N.U. Wetter, J.J. Neto, Effect of the ytterbium concentration on the upconversion luminescence of Yb3+/Er3+ co-doped PbO–GeO2–Ga2O3 glasses, J. Non-Cryst. Solids 354 (2008) 4755–4759.
[9] D.S. Da Silva, L.P. Naranjo, L.R.P. Kassab, C.B. De Araújo, Photoluminescence from germanate glasses containing silicon nanocrystals and erbium ions, Appl. Phys. B Laser Opt. 106 (2012) 1015–1018, https://doi.org/10.1007/s00340-011-4798-3.
[10] D.S. Da Silva, Thiago A.A. De Assumpção, Giordano B.C. De Simone, L.R.P. Kassab, Cid B. De Araújo, Enhanced Er 3+ photoluminescence in TeO 2 –ZnO glass containing silicon nanocrystals, Appl. Phys. B 121 (2015) 117–121, https://doi.org/10.1007/s00340-015-6207-9.
[11] D.S. Wiersma, The physics and applications of random lasers, Nat. Phys. 4 (2008) 359–367, https://doi.org/10.1038/nphys971.
[12] E. Jimenez-Villar, V. Mestre, P.C. de Oliveira, G.F. de Sá, Novel core–shell (TiO2@Silica) nanoparticles for scattering medium in a random laser: higher efficiency, lower laser threshold and lower photodegradation, Nanoscale 5 (2013) 12512, https://doi.org/10.1039/c3nr03603k.
[13] E. Jimenez-Villar, V. Mestre, P.C. De Oliveira, W.M. Faustino, D.S. Silva, G.F. De Sá, TiO2@Silica nanoparticles in a random laser: strong relationship of silica shell thickness on scattering medium properties and random laser performance, Appl. Phys. Lett. 104 (2014) 2–7, https://doi.org/10.1063/1.4865092.
[14] E. Jiménez-Villar, I.F.I.F. Da Silva, V. Mestre, N.U.N.U. Wetter, C. Lopez, P.C.P.C. De Oliveira, W.M.W.M. Faustino, G.F.G.F. De Sá, Random lasing at localization transition in a colloidal suspension (TiO2@Silica), ACS Omega 2 (2017) 2415–2421, https://doi.org/10.1021/acsomega.7b00086.
[15] N.U. Wetter, J.M. Giehl, F. Butzbach, D. Anacleto, E. Jiménez-Villar, Polydispersed powders (Nd 3+ :YVO 4) for ultra efficient random lasers, Part. Part. Syst. Char. (2017) 1700335, https://doi.org/10.1002/ppsc.201700335.
[16] N.U. Wetter, A.R. de Miranda, É. Pecoraro, S.J.L. Ribeiro, E. Jimenez-Villar, Dynamic random lasing in silica aerogel doped with rhodamine 6G, RSC Adv. 8 (2018) 29678–29685.
[17] S. John, Electromagnetic absorption in a disordered medium near a photon mobility edge, Phys. Rev. Lett. 53 (1984) 2169–2172, https://doi.org/10.1103/PhysRevLett.53.2169.
[18] E. Jimenez-Villar, I.F. Da Silva, V. Mestre, P.C. De Oliveira, W.M. Faustino, G.F. De Sá, Anderson localization of light in a colloidal suspension (TiO2@silica), Nanoscale 8 (2016) 10938–10946, https://doi.org/10.1039/c5nr07540h.
[19] E. Jimenez-Villar, V. Mestre, W.S. Martins, G.F. Basso, I.F. Da Silva, G.F. De Sá, Core-shell TiO2@Silica nanoparticles for light confinement, Mater. Today Proc. 4 (2017) 11570–11579, https://doi.org/10.1016/j.matpr.2017.09.068.
[20] E. Jimenez Villar, M.C.S. Xavier, J.G.G.S. Ramos, N.U. Wetter, V. Mestre, W.S. Martins, G.F. Basso, V.A. Ermakov, F.C. Marques, G.F. de Sá, Localization of light: beginning of a new optics, in: D.L. Andrews, E.J. Galvez, J. Glückstad (Eds.), Complex Light Opt. Forces XII, Proceeding SPIE 10549, 2018, p. 1054905, https://doi.org/10.1117/12.2288993.
[21] E. Jimenez-Villar, M.C.S. Xavier, N.U. Wetter, V. Mestre, W.S. Martins, G.F. Basso, V.A. Ermakov, F.C. Marques, G.F. de Sá, Anomalous transport of light at the phase transition to localization: strong dependence with incident angle, Photon. Res. 6 (10) (2018) 929–942.
[22] S. John, Strong localization of photons in certain disordered dielectric superlattices, Phys. Rev. Lett. 58 (1987) 2486–2489, https://doi.org/10.1103/physrevlett.58.2486.
[23] S. John, J. Wang, Quantum electrodynamics near a photonic band gap: photon bound states and dressed atoms, Phys. Rev. Lett. 64 (1990) 2418–2421, https://doi.org/10.1103/physrevlett.64.2418.
[24] S. John, Localization of light, Phys. Today 44 (1991) 32–40, https://doi.org/10.1063/1.881300.
[25] Y. Wu, Y. Ren, A. Chen, Z. Chen, Y. Liang, J. Li, G. Lou, H. Zhu, X. Gui, S. Wang, Z. Tang, A one-dimensional random laser based on artificial high-index contrast scatterers, Nanoscale 9 (2017) 6959–6964, https://doi.org/10.1039/c7nr00261k.
[26] F.A. Bomfim, D.M. Da Silva, L.R.P. Kassab, T.A.A. De Assumpção, V.D. Del Cacho, M.I. Alayo, Advances on the fabrication process of Er3+/Yb3+:GeO2-PbO pedestal waveguides for integrated photonics, Opt. Mater. (Amst.) 49 (2015) 196–200, https://doi.org/10.1016/j.optmat.2015.09.010.
[27] M. Miritello, P. Cardile, R. Lo Savio, F. Priolo, Energy transfer and enhanced 154 $\upmu$m emission in Erbium-Ytterbium disilicate thin films, Opt. Express 19 (2011) 20761, https://doi.org/10.1364/oe.19.020761.
[28] T.A.A. de Assumpção, M.E. Camilo, M.I. Alayo, D.M. da Silva, L.R.P. Kassab, Influence of gold nanoparticles on the 805 nm gain in Tm3+/Yb3+codoped PbO-GeO2pedestal waveguides, Opt. Mater. (Amst.) 72 (2017) 518–523, https://doi.org/10.1016/j.optmat.2017.06.031.
[29] P. Goodhew, General introduction to transmission electron microscopy ({TEM}), in: Aberration-Corrected Anal. Transm. Electron Microsc., John Wiley & Sons, Ltd, 2011, pp. 1–19, https://doi.org/10.1002/9781119978848.ch1.
[30] N. Dai, B. Xu, Z. Jiang, J. Peng, H. Li, H. Luan, L. Yang, J. Li, Effect of Yb^3$\mathplus$ concentration on the broadband emission intensity and peak wavelength shift in Yb/Bi ions co-doped silica-based glasses, Opt. Express 18 (2010) 18642, https://doi.org/10.1364/oe.18.018642.
[31] A. Winterstein, S. Manning, H. Ebendorff-Heidepriem, L. Wondraczek, Luminescence from bismuth-germanate glasses and its manipulation through oxidants, Opt. Mater. Express 2 (2012) 1320, https://doi.org/10.1364/ome.2.001320.
[32] M. Peng, N. Zhang, L. Wondraczek, J. Qiu, Z. Yang, Q. Zhang, Ultrabroad NIR luminescence and energy transfer in Bi and Er/Bi co-doped germanate glasses,

Opt. Express 19 (2011) 20799, https://doi.org/10.1364/OE.19.020799.
[33] J. Qiu, M. Peng, J. Ren, X. Meng, X. Jiang, C. Zhu, Novel Bi-doped glasses for broadband optical amplification, J. Non-Cryst. Solids 354 (2008) 1235–1239, https://doi.org/10.1016/j.jnoncrysol.2007.02.094.
[34] R. Swanepoel, Determination of the thickness and optical constants of amorphous silicon, J. Phys. Educ. 16 (1983) 1214–1222, https://doi.org/10.1088/0022-3735/16/12/023.
[35] (n.d.), http://omlc.org/calc/mie_calc.html.
[36] C. Strohhöfer, A. Polman, Relationship between gain and Yb3+ concentration in Er3+-Yb3+ doped waveguide amplifiers, J. Appl. Phys. 90 (2001) 4314–4320, https://doi.org/10.1063/1.1406550.
[37] L. Pavesi, R. Turan, Silicon Nanocrystals: Fundamentals, Synthesis and Applications, 2010, https://doi.org/10.1002/9783527629954.